Thermospheric Temperature and Density Variability During 3–4 February 2022 Minor Geomagnetic Storm

F. I. Laskar[1] , E. K. Sutton[2] , D. Lin[3] , K. R. Greer[1] , S. Aryal[1] , X. Cai[1] , N. M. Pedatella[3] , R. W. Eastes[1] , W. Wang[3] , M. V. Codrescu[4], and W. E. McClintock[1]

[1]Laboratory for Atmospheric and Space Physics, University of Colorado Boulder, Boulder, CO, USA, [2]Space Weather Technology, Research, and Education Center (SWx TREC), University of Colorado Boulder, Boulder, CO, USA, [3]High Altitude Observatory, National Center for Atmospheric Research, Boulder, CO, USA, [4]Space Weather Prediction Center, NOAA, Boulder, CO, USA

Abstract Themospheric conditions during a minor geomagnetic event of 3 and 4 February 2022 has been investigated using disk temperature (T_{disk}) observations from Global-scale Observations of the Limb and Disk (GOLD) mission and model simulations. GOLD observed that the T_{disk} increases by more than 60 K during the storm event when compared with pre-storm quiet days. A comparison of the T_{disk} with effective temperatures (T_{eff}, i.e., a weighted average based on airglow emission layer) from Mass Spectrometer Incoherent Scatter radar version 2 (MSIS2) and Multiscale Atmosphere-Geospace Environment (MAGE) models shows that MAGE outperforms MSIS2 during this particular event. MAGE underestimates the T_{eff} by about 2%, whereas MSIS2 underestimates it by 7%. As temperature enhancements lead to an expansion of the thermosphere and resulting density changes, the value of the temperature enhancement observed by GOLD can be utilized to find a GOLD equivalent MSIS (GOLD-MSIS) simulation—from a set of MSIS2 runs obtained by varying geomagnetic ap index values. From the MSIS-GOLD run we found that the thermospheric density enhancement varies with altitude from 15% (at 150) to 80% (at 500 km). Independent simulations from the MAGE model also show a comparable enhancement in neutral density. These results suggest that even a modest storm could impact the thermospheric densities significantly and GOLD data can be used to improve the empirical and assimilative models of the thermosphere.

Plain Language Summary High speed plasma from the sun can bring energy, momentum, and particles into the Earth's upper atmosphere triggering a geomagnetic storm, which disturbs the thermosphere-ionosphere (TI) system. It is observed that even minor geomagnetic events can have a significant impact on the TI system. In this work we have investigated the neutral properties of the thermosphere during a minor geomagnetic event using NASA-Global-scale Observations of the Limb and Disk (GOLD) mission observations. By calibrating the Mass Spectrometer Incoherent Scatter radar version 2 empirical model based on the temperature change observed by GOLD, we have found that the thermospheric density increased by 15% (at 150) to 80% (at 500 km). These results demonstrates that the GOLD data can help in improving thermospheric empirical models. Also, they can help satellite-drag and space weather forecasters to find ways to improve their products.

1. Introduction

The Thermosphere-Ionosphere (TI) system of the Earth is externally forced by waves from the lower atmosphere and energy and momentum inputs from the sun through solar irradiance and solar wind energetic particles. The solar irradiance controls the thermospheric background neutral density and temperature through heating by the extreme ultraviolet radiation, one form of solar forcing. Another form of solar forcing comes from solar energetic charged particles from coronal mass ejection, high-speed streams, and corotating interaction regions. These charged particles behave like a plasma and are termed as the solar wind. The solar wind magnetic field, depending on its directionality, reconnects with Earth's magnetic field, transporting the solar wind energetic charged particles into the Earth's magnetosphere. Due to magnetosphere and ionosphere coupling through precipitation and electric fields, currents and resulting joule heating are produced, which perturbs the TI system. These perturbations then spread globally transporting energy and momentum. The transport happens through a high to lower latitude circulation induced by the heating and through Traveling Atmospheric Disturbance, that transports energy into the mid- to low-latitudes (Burns et al., 1995). Depending on the storm strength it can take from ~3 hr

to tens of hours for the high-latitude heating to reach low-latitudes (Oliveira & Zesta, 2019; Sutton et al., 2009; Zesta & Oliveira, 2019).

Perturbations can also be generated by waves propagating upwards from the lower atmosphere and by solar transient events like solar flares, but the main aim of the current investigation is to study the perturbations during geomagnetic storms. The above description is a simple picture of the solar wind-magnetosphere-ionosphere-thermosphere connection. For a detailed description one can see some review articles by Akasofu (1981) and Richmond and Lu (2000). These perturbations in thermospheric temperature and neutral density can disrupt the ionospheric communications and satellite-based navigation, which could potentially be a factor of great economic loss (Berger et al., 2020; Eastwood et al., 2017). With the rise of private sector space exploration industries that are launching thousands of satellites for megaconstellations, it is crucial to understand the physical processes and to improve forecast of the TI system (Berger et al., 2020; Jackson et al., 2019).

Though there occurs energy deposition primarily at auroral latitudes, the energy is transported even to the mid- and low-latitudes through waves and thermal advection, which eventually enhances the global temperature (Laskar, Eastes, et al., 2021; Richmond, 2021). However, in some storms the thermosphere exhibits overcooling and contraction after a main-phase heating. This occurs when excessive particle precipitation enhances the concentration of nitric oxide, a radiative cooling agent, in the thermosphere (Knipp et al., 2017). But, for the current case we are dealing with the net effect that is mostly heating (Laskar, Eastes, et al., 2021). The enhanced temperature leads to thermospheric density increase at a given altitude (e.g., T. J. Fuller-Rowell et al., 1994; Prölss, 2010; Richmond, 2021). The resultant enhanced density leads to larger satellite drag, particularly for the Low-Earth-Orbit (LEO) satellites (Li & Lei, 2021; Sutton et al., 2005).

Most of the earlier studies have concentrated on the impact of major storms on the thermosphere using either satellite based upper thermospheric neutral densities or lower thermospheric temperature (e.g., Bruinsma et al., 2006; H. Liu & Lühr, 2005; R. Liu et al., 2010; Sutton et al., 2005; Yuan et al., 2019). But in recent times, with the availability of synoptic and rich local time temperature and composition data that are representative of a unique region, the middle thermosphere, from Global Scale Observations of the Limb and Disk (GOLD), it has been observed that even minor storms (with ap index less than 14 nT) can also impact the thermosphere significantly (Aa et al., 2021; Cai, Burns, Wang, Qian, Pedatella, et al., 2021; Cai, Burns, Wang, Qian, Solomon, et al., 2021; Laskar, Eastes, et al., 2021). An example of the consequences of such increases in satellite drag during a modest storm is the loss of 38 out of 49 satellites during the 38th launch of the SpaceX's Starlink constellation (Hapgood et al., 2022). The impact of these minor storms are not well represented in physics based general circulation models (GCM). For space weather forecasting such models are used as background model, that are used to get an initial condition or forecast ensemble by advancing the model to next assimilation time-step. Therefore, for a better predictive capability of the thermospheric density and drag, which are critical for satellite traffic control, it is crucial that the impact of these storms be well understood and captured in existing whole atmosphere GCM and empirical models (Jackson et al., 2019). Whole atmosphere data assimilation using existing and upcoming ground and satellite based TI system measurements would be of help toward development of a better monitoring and predictive capability of space weather (Berger et al., 2020; Jackson et al., 2019; Laskar, Pedatella, et al., 2021; Laskar et al., 2022; Mlynczak et al., 2018).

Earlier investigations using thermospheric density measurements from LEO satellites have provided results on the density enhancement during geomagnetic storm events (e.g., Crowley et al., 2006; Forbes et al., 1996; Sutton et al., 2005). But those were carried out either using upper or lower thermospheric neutral observations. Also, the exact mechanisms through which the temperature and density perturbations distribute at different altitudes and over the globe are still being investigated. It is not always true that the temperature and density enhancements occur at the exact location where the Joule heating occurs. In fact it has been observed that the temperature increase happens globally but larger enhancements in temperature occur at higher latitudes (Laskar, Eastes, et al., 2021). Moreover, as geomagnetic storm events change the thermospheric circulation, the largest temperature enhancements occur mostly in regions where the horizontal motion of the air converges, which occurs mostly in the prenoon local times (Burns et al., 1995; Laskar, Eastes, et al., 2021).

The current capabilities of estimating the thermospheric neutral density and temperature using empirical models are generally good on the global average, but their estimation abilities are limited and they cannot forecast the spatial structures and conditions, particularly during a geomagnetic storm (Berger et al., 2020; Jackson et al., 2019). Recent progress in physics based whole geospace modeling (e.g., Multiscale Atmosphere Geospace

Environment [MAGE]) show substantial improvements in characterizing storm time thermospheric density compared to standalone GCM (Pham et al., 2022). Note that a whole geospace model is a two-way coupled magnetosphere-ring current-ionosphere-thermosphere model that solves for the physical interactions between the solar wind and the magnetosphere-ionosphere-thermosphere system and the coupling processes within the geospace. However, the knowledge gained from currently available satellite based measurements have potential to improve results from the empirical models. Also, incorporating the current observations in a whole atmosphere assimilation and forecasting system could potentially improve the current understanding of the TI system (Laskar et al., 2022). Moreover, the altitudes lower than 200 km are below the reach of in situ satellite measurements, and remote sensing of the altitudes between 120 and 250 km has been rare (Forbes et al., 1996). In this investigation we use data from NASA's GOLD mission to study a minor geomagnetic event and show that their use improves the thermospheric empirical model results, providing a better understanding of the storm time TI system. A quantification of the thermospheric temperature changes in response to the storm has been made with GOLD data, which is then simulated in an empirical model to quantify the vertical profiles of the thermospheric density changes. The results are then compared with a state-of-the-art magnetosphere-ionosphere-thermosphere coupled model simulation (in this case, MAGE). The prime purpose of the present investigation is to demonstrate that the GOLD temperature ingestion into an existing empirical model improves our understanding of the thermospheric conditions during a minor geomagnetic storm by improving representation of the temperature and density variability. Our results demonstrate a methodology for the improvement of operational satellite drag products.

2. Data, Model, and Methodology

GOLD disk temperature T_{disk} is compared with predictions from the Mass Spectrometer Incoherent Scatter-radar version 2 (MSIS2) and MAGE models. The MSIS2 is forced with different level of geomagnetic activity to simulate a GOLD T_{disk} equivalent run. The MAGE model is used to compare its densities with the GOLD informed MSIS2 calculations. Further details of these data and models are given below.

2.1. GOLD T_{disk}

GOLD observes the Earth's disk and limb in the FUV for over 18.5 hr each day, from 06:10 to 00:40 universal time (UT) of the next day (Eastes et al., 2019, 2020; Laskar et al., 2020; McClintock et al., 2020). The daytime disk measurements cover about 06:10–23:00 UT. GOLD daytime disk scans of the N_2 Lyman-Birge-Hopfield (LBH) bands are used to retrieve the T_{disk} data. As the GOLD N_2 LBH emissions are column integrated quantities, the retrieved T_{disk} products are a representative of the corresponding N_2 LBH layer. The peak altitude of the layer has a range of 150–220 km which varies with solar zenith angle (SZA) and emission angle. But the peak altitudes remain below 200 km for all SZA and emission angles less than 70° (Evans et al., 2018; Laskar, Pedatella, et al., 2021). GOLD scans each full disk in about 30 min. The T_{disk} retrieval algorithm is an improvement of the code that was used previously to derive temperature from limb measurements of N_2 LBH intensity from the High-resolution Ionospheric and Thermospheric Spectrograph instrument (Aksnes et al., 2006; Evans et al., 2018; Krywonos et al., 2012). Effective neutral temperatures are retrieved by fitting the observed rotational structure of the N_2 LBH bands using an optimal estimation routine (Evans et al., 2018; Lumpe et al., 2002; Rodgers, 2000). The current investigation used Level 2 (L2) T_{disk} version 3 (V03) data that are retrieved from 2×2 binned level-1C N_2 LBH spectra, which are available at the GOLD web-page, https://gold.cs.ucf.edu/ as "Level 2—TDISK." The 2×2 binned data have a spatial resolution of 250×250-km near nadir. Typical random errors in the 2×2 binned T_{disk} data varies with signal-to-noise ratio (SNR) of the N_2 LBH emission and it ranges from 20 (for high SNR) to 90 K (for low SNR).

2.2. NRLMSIS2.0 Model

Naval Research Laboratory MSIS2.0 (NRLMSIS2.0) is an empirical model of the thermosphere. The earlier versions of MSIS (MSIS-86 and MSIS-90) simulated neutral composition, total mass density, and temperature (Hedin, 1987, 1991). MSIS-86 was available for altitudes above 90 km, whereas MSIS-90 was extended from the ground to the exobase (Hedin, 1991). Later development led to the NRLMSISE-00 which improved the total mass density by incorporating more orbital drag and accelerometer data (Picone et al., 2002). Recently, the model was further updated to NRLMSIS2.0 (Emmert et al., 2021) and NRLMSIS2.1 (Emmert et al., 2022). In this

version, extensive new data were incorporated to estimate the profiles of neutral temperature, 8 neutral species densities, and total neutral mass density based on, time, location, solar activity, and geomagnetic activity. Emmert et al. (2021) noted relatively lower predicted temperature in this iteration of the model compared to its predecessor, which likely affects the neutral densities. NRLMSIS 2.0 densities are fully coupled to temperature from the ground to the exosphere via a hydrostatic/diffusive equilibrium profile (see Emmert et al. (2021)). We have used the latest iteration, NRLMSIS2, here onward we refer it as MSIS2. A python wrapper of the original Fortran code was used to run the model (Lucas, 2021).

The inputs to the standard MSIS2 are UT time, day of year, geomagnetic ap index, solar F10.7 cm flux, and 81-day averaged solar F10.7 cm flux. In the present investigation, we have used the geomagnetic indices in MSIS2 in two different ways: (a) MSIS2 with observed geomagnetic ap index, a single 3-hourly ap value coincident in time with the simulated thermosphere, referred to as MSIS2 and (b) ap adjusted MSIS2, referred to as MSIS-GOLD. The ap adjustment in the second case is obtained by parameterizing the ap index based on the observed GOLD-temperature data, further details are given in the seventh paragraph of the results section. For the present investigation, even if we use seven different types of ap values (Hedin, 1987) for the case (a), the results are very comparable (not presented here) to that obtained from single 3-hourly instantaneous ap indices.

2.3. MAGE Model

MAGE couples multiple models of the magnetosphere, the ring current, and the ionosphere-thermosphere into a coherent two-way coupling scheme. The model couples Grid Agnostic Magnetohydrodynamic model for Extended Research Applications global model of magnetosphere (Sorathia et al., 2020), the Rice Convection Model of ring current (RCM, Toffoletto et al. (2003)), the Thermosphere-Ionosphere Electrodynamics General Circulation Model (TIEGCM, L. Qian et al. (2014); Richmond et al. (1992)), and the RE-developed Magnetosphere-Ionosphere Coupler/Solver, which is a rewrite of the MIX code (Merkin & Lyon, 2010). Greater details of the coupling schemes, preliminary validation of some of the states, and the working principle can be found in Lin et al. (2021) and Pham et al. (2022). The MAGE model has been widely used in a number of storm time ionosphere-thermosphere studies (Lin, Wang, Garcia-Sage et al., 2022), and various states of it are found to compare well with observational data (Lin, Wang, Merkin, et al., 2022; W. Qian et al., 2022; Shi et al., 2022).

3. A Recent Geomagnetic Event and Its Significance

On 03 February 2022 there was a geomagnetic storm, for which some of the geomagnetic parameters are shown in Figure 1. The storm started at about 00:00 UT on 03 February (as depicted by the vertical dashed-line) and was strengthened for a second time near 00:00 UT on 04 February with an active phase lasting the whole day. The shaded region in Figure 1 represents the active days when z component of Interplanetary Magnetic Field (IMF Bz) was mostly southward, relatively faster solar wind, and two episodes of Dst index reaching down to −65 nT. Notably, on 03 February SpaceX launched 49 satellites to very low earth orbits (VLEO, about 210 km) in preparation to boost individual satellites into a higher operating orbit, of which 38 were lost due to an unusual increase in the satellite drag (Hapgood et al., 2022), which SpaceX reported to be about 50% higher compared to their previous experiences during low solar and quiet geomagnetic conditions. This event motivated us to investigate the thermospheric conditions using GOLD data and model simulations. This study is focused on characterizing the thermospheric conditions on these 2 days.

Based on the Dst index this storm could be classified as "moderate" storm (Borovsky & Shprits, 2017; Loewe & Prölss, 1997). As Dst is not always a great indicator of geospace storm (Borovsky & Shprits, 2017; McPherron & Chu, 2016), we also use National Oceanic and Atmospheric Administration's (NOAA) Space Weather Prediction Center (SWPC) classification. The highest 3 hourly Kp and ap indices during this event were 5+ and 56 nT (Figure 1d), respectively. Based on the NOAA SWPC Space Weather Scales (https://www.swpc.noaa.gov/sites/default/files/images/NOAAscales.pdf) classification this storm is a minor (G1 class) event. So, we designate this as a "minor" event.

4. Results

4.1. Results From GOLD Observations

Figure 2 shows the observations of the GOLD disk temperatures (T_{disk} in Figures 2a–2d) and difference from a quiet day Figures 2e–2h on 03 February 2022, when there was a minor geomagnetic storm. A 4 × 4 pixel (about
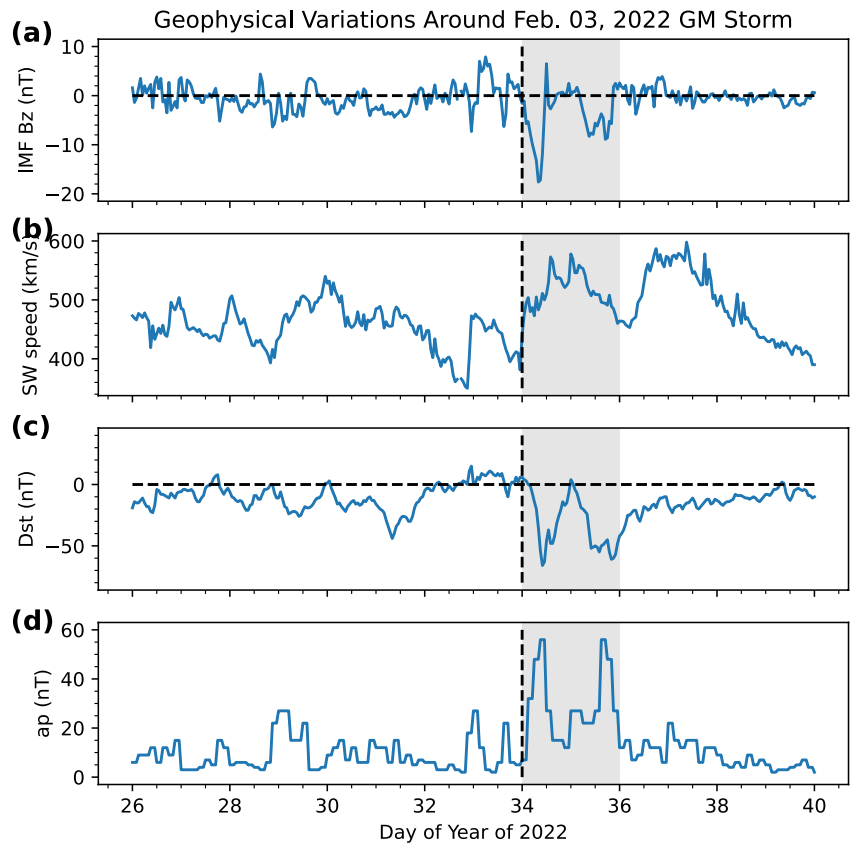
Figure 1. Geomagnetic indices and solar wind conditions in-and-around the 03 February 2022 minor geomagnetic storm. The shaded region represents the active days with Interplanetary Magnetic Field Bz mostly southward, relatively faster solar wind, and two episodes of Dst reaching below −50 nT.
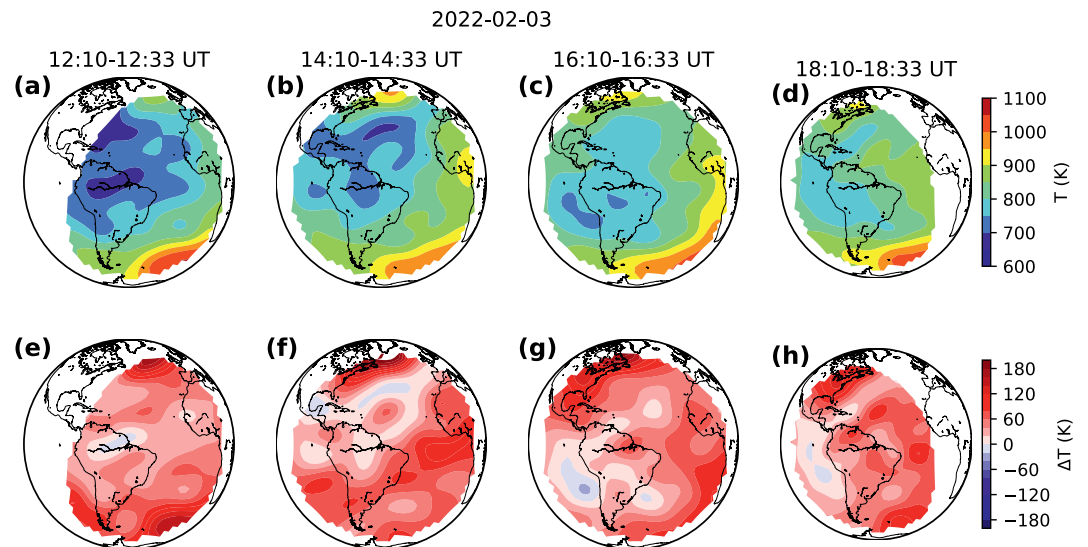
Figure 2. T_{disk} (referred to as T here, "a"–"d") and difference from quiet time (ΔT, "e"–"h") on 03 February 2022 are shown. The bottom panels show a mostly positive ΔT, suggesting an overall increase in the thermospheric temperature with respect to the pre-storm reference.

Figure 3. Day-to-day and latitudinal variability of the Global Scale Observations of the Limb and Disk disk temperatures averaged between 40° and 53°W in and around the geomagnetic storm on 03 and 04 February 2022. An increase in temperature can be noted from day 34, when there was a geomagnetic storm as can be seen from the 30 min cadence ap index values.

1,000 km) smoothing of the temperature data are carried out to generate smooth looking images as presented in Figure 2. The background or baseline values, that are used to calculate differen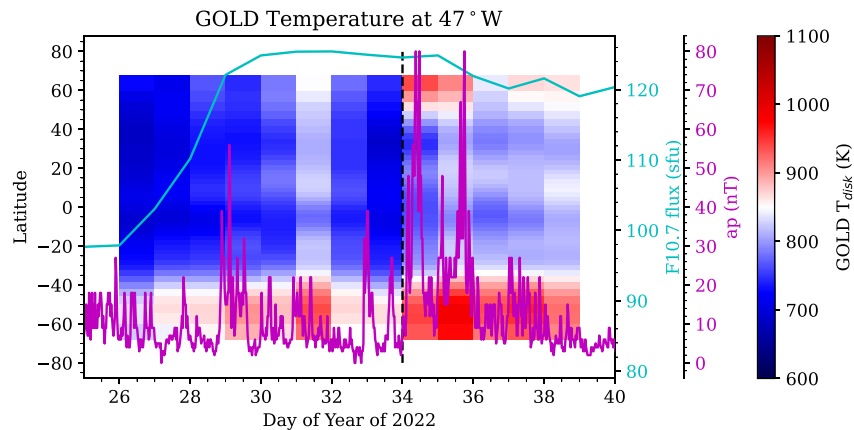ce, are approximated by taking the average of the four days of T_{disk} data from 26–30 January 2022. The four days are chosen in such a way that the geomagnetic activity was quiet, so we excluded 29 January 2022, which was a slightly disturbed day. Also, averaging the disks over four days reduces the day-to-day variability and the random noise, which varied from 20 to 90 K for a particular disk image, depending on the SNR of the LBH emissions measured at that location (Laskar et al., 2022). From the differences (ΔT) it can be noted that the values are positive over the majority of the disk on the storm day.

To investigate how the temperatures varied prior to, during, and after the geomagnetic storm, the day-to-day and latitudinal variations of the T_{disk} averaged over 40°–53°W longitude region and for UTs of the four full disk scans (that are shown in Figure 2) are shown in Figure 3 along with the solar F10.7 cm flux and 30 min cadence geomagnetic ap index (Matzka et al., 2022; Yamazaki et al., 2022). Again, the temporal and spatial averaging is done to reduce the random noise in the GOLD T_{disk}. The temperature starts to increase from the day-of-year (DOY) 34, when there happened a geomagnetic storm starting very early in the morning of 03 February 2022 as can be seen from the ap index in Figure 1 or 30-min ap from Figure 3. The unusual increase at every latitude on 31 January was caused by an increased radiation level at the geostationary altitudes, as observed by the detector radiation counts (shown in Figure S2 in Supporting Information S1). Such enhanced radiation degraded the signal to noise and therefore the temperature bias in the retrieval. But this does not impact the results and is not of interest for the current study. Also, it can be stated it is not an effect of geomagnetic activity as that day was relatively quiet.

The enhanced temperature over all the days at southern mid- and high-latitudes (above 40°S) is due to seasonal variation, summer in the southern hemisphere. This enhanced temperature gets further enhanced on the storm days (day 34–35). As the neutral density at those altitudes is proportional to temperature, the SpaceX satellites could have experienced increased drag. But the perigee of the launch was in the northern mid-latitude on the storm days and at the latitudes south of 40°S the satellites were at about 260 km altitude, more than a scale height higher than perigee (~210 km), therefore they would have had less of an impact to the overall satellite drag. Perigee locations and altitudes of a sample pass are shown in Figure S1 in Supporting Information S1. Note that GOLD scans the whole disk in 30 min, so we use the 30-min cadence ap indices for better comparison. But for this figure, even though 30 min cadence ap is not important we keep them to show that even the high-cadence ap does not exceed 80 nT on the storm day. In this investigation 30-min ap is used in this figure only, but in other places ap refers to 3-hr cadence geomagnetic ap index that are presented in Figure 1.

To calculate the average increase in temperature over the disk, the four full-disk scans of data as shown in Figure 2 are averaged (arithmetic mean) for the two storm days (3 and 4 February) and a similar averaging is done for the baseline quiet day (in this Case 1 February 2022). For this study we are providing the global (all latitude) average picture to put them in the context of earlier studies where LEO orbit averaged pictures were presented (Dang et al., 2022; Sutton et al., 2009). However, GOLD does have greater potential to demonstrate spatial and
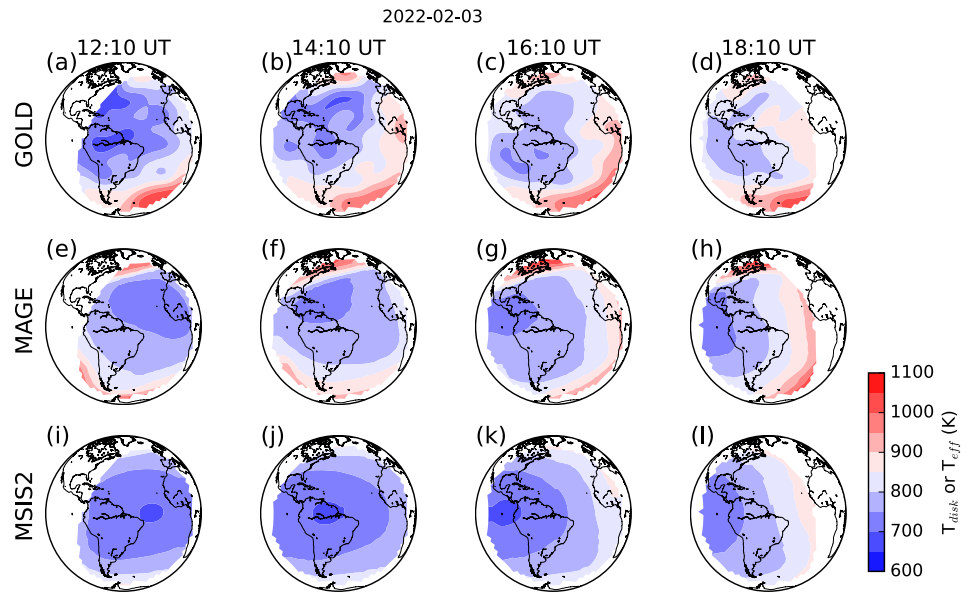
Figure 4. (a–d) Global Scale Observations of the Limb and Disk (GOLD) T_{disk} for the four disk scans on the storm day, (e, f) GOLD equivalent effective temperature (T_{eff}) from the Multiscale Atmosphere-Geospace Environment (MAGE) model, and (i–l) GOLD equivalent effective temperature (T_{eff}) from Mass Spectrometer Incoherent Scatter-radar version 2 (MSIS2). Notable features are that the GOLD and MAGE-T_{eff} are in good agreement but the MSIS2 underestimate the T_{eff}.

temporal variations over the disk to investigate storm time thermospheric variability, which could be demonstrated in further studies for particular locations/orbit passing through the disk. Considering the 1 February as the baseline day, the temperature difference between active and quiet times is about 61 K, with errors below 1 K as the calculations are done with more than four thousand data points over the disk. Note that the ΔT values are subject to the reference day being selected but for all possible quiet days within 26 January–2 February the values vary from 47 K (with 31 January as baseline) to 95 K (with 26 January as baseline). Note that the 61 K increase in T_{disk} and the range of this increase (47–95 K, with respect to other baselines) are the primary findings from GOLD and they will be used later for estimations of thermospheric density perturbations at different altitudes.

4.2. Results From Model Simulations

As presented above, we have made an estimate of the lower- and middle-thermospheric T_{disk} enhancement during the storm event. To estimate the corresponding thermospheric density changes in response to the geomagnetic storm, we have used two different simulation approaches. (a) an empirical method in which MSIS2 was used to simulate thermospheric conditions that are equivalent to GOLD temperature increase and (b) MAGE model simulations. The MAGE model is used for an independent comparison of the calculations made using MSIS2 assisted with knowledge gained from GOLD (here onward we refer this as MSIS-GOLD). As mentioned above, from GOLD we have observed a temperature increase of about 61 K when averaged over the GOLD field of view. This temperature enhancement can expand the thermosphere and give rise to density increase at a given altitude. To find out how much the thermospheric density will change in response to this T_{disk} increase MSIS2 simulations are carried out.

Before we estimate the density changes with MSIS2, let us see how the GOLD T_{disk} compare with MSIS2 and MAGE temperatures. GOLD equivalent temperatures (T_{eff}) are calculated from MSIS2 and MAGE using contribution functions as reported in Laskar, Pedatella, et al. (2021), a two-dimensional plot of this is given in Figure S3 in Supporting Information S1. The contribution function used here is a function of altitude and SZA. The function shape is based on the LBH airglow layer shape which ranges from ~100 to ~400 km and maximizes at around 160 km (Laskar, Pedatella, et al., 2021). Model temperature profiles are multiplied by the normalized contribution function and then integrated in altitude to get the effective temperature. Figure 4 shows the comparison plots for the four disk scans taken on the storm day, 03 February 2022. It can be seen that the MSIS2-T_{eff} is smaller than GOLD, and the MAGE-T_{eff} is in better agreement with GOLD T_{disk}. The percentage deviations of

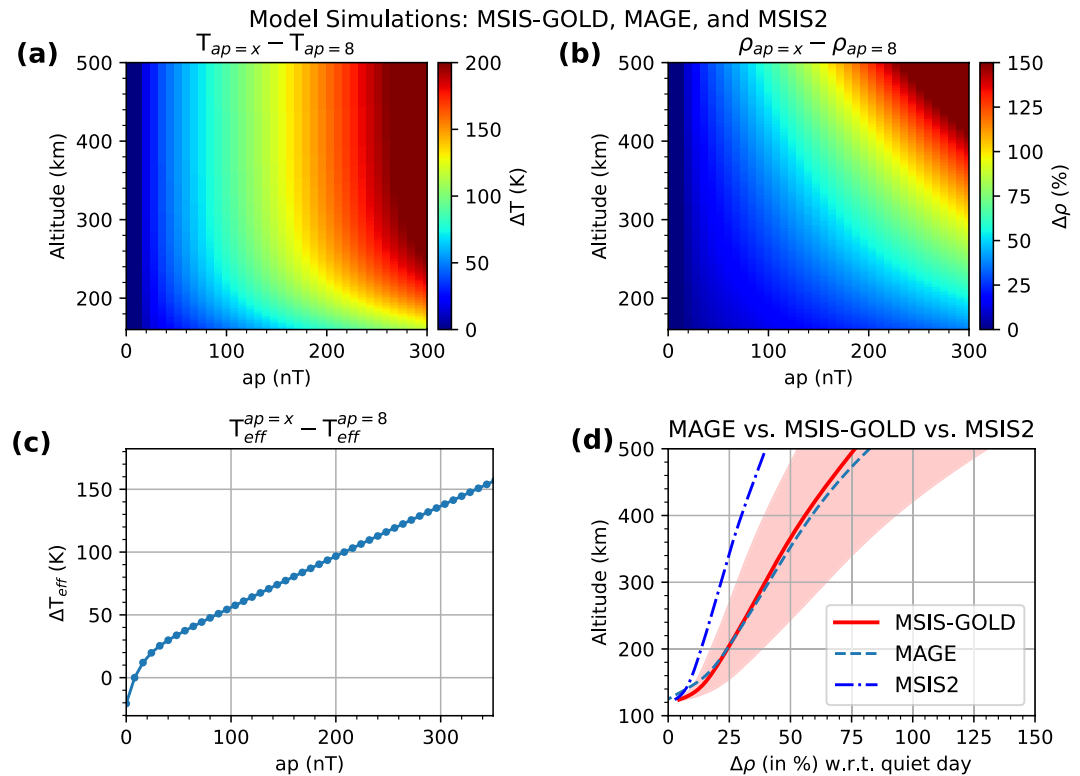## Model Simulations: MSIS-GOLD, MAGE, and MSIS2

Figure 5. Mass Spectrometer Incoherent Scatter-radar version 2 (MSIS2) model simulation of thermospheric temperature difference (a) and percentage change in neutral density (b) in response to changing geomagnetic activity levels (varied ap indices). MSIS2 effective temperature differences (c) with respect to ap = 8 level and the altitude variation of density for an ap level of 116 nT (d). The ap = 116 nT corresponds to a ΔT_{eff} of 61 K. Panel (d) shows the range of densities with upper and lower bounds of the pink shaded region correspond to MSIS-Global Scale Observations of the Limb and Disk with $\Delta T_{eff} = 47$ (lower bound) and $\Delta T_{eff} = 95$ K (upper bound). Multiscale Atmosphere-Geospace Environment simulation and MSIS2 model simulated percentage density differences are also shown in panel (d).

model temperatures with respect to T_{disk} are about 6.9% for MSIS2 and 2.3% for MAGE, which suggests that the thermospheric temperatures are underestimated in both MSIS2 and MAGE.

Though MSIS2 underestimates the thermospheric temperature when compared with GOLD, the model can be tuned to investigate how much density change can happen in response to a change in T_{eff}. Therefore, we use MSIS2 to estimate the change in thermospheric neutral density in response to the 61 K increase observed in GOLD T_{disk}. Being an empirical model, MSIS2 can be forced with various geomagnetic conditions to see their impact on the thermospheric temperature and neutral density. So, we have used a set of geomagnetic ap indices ranging from 0 to 390 nT, with a step size of 8 nT, to find out what level of geomagnetic activity (or ap) is needed to observe a T_{eff} difference that is the same as that observed from GOLD (61 K as mentioned above). Figure 5a shows the temperature difference between different MSIS2 runs with varied ap index. To calculate the perturbations, MSIS2 simulation states corresponding to an ap value of 8 nT has been used as the baseline. This is because, an earlier study by Laskar, Eastes, et al. (2021) has shown that the base level of geomagnetic activity that does not perturb the thermospheric temperature is about 8 nT. Other input parameters, such as, UT, geo-location, F10.7 and F10.7A are set at 15:00 UT, 60°N–60°S and 48°W, 100, and 100 sfu, respectively. Note 1 sfu = 10^{-22} W m^{-2} Hz^{-1} and 48°W longitude is choosen as it is the sub-satellite longitude of GOLD. The latitude and altitude resolutions of MSIS2 are 5° and 2 km. For the presentation in Figure 5, a latitude average of all the runs is shown to have a similar averaging as that was done for the GOLD data. From the temperature differences (in Figure 5a), it can be seen clearly that with increasing geomagnetic activity the thermospheric temperatures increase, also the corresponding density differences (in Figure 5b) are positive and increasing with increasing geomagnetic activity level.

To further quantify the thermospheric conditions the effective temperatures averaged over 60°N–60°S are shown in Figure 5c for the ap indices considered. From Figure 5c we can estimate that an ap index of 116 nT is needed, which is about 60 nT higher than the maximum 3 hourly ap value observed on that day, for MSIS2 to reproduce a

T_{eff} difference of 61 K. We have also identified the MSIS2 simulations for which the effective temperature differences are 47 (ap = 82) and 95 K (ap = 202 nT). The neutral density enhancements for the simulations with T_{eff} differences of 61 (or, ap = 116), 47 (or, ap = 82), and 95 K (or, ap = 202 nT) are shown in Figure 5d. The region between density differences corresponding to T_{eff} differences of 47 and 95 K are shown as shadowed region. Hence, the density difference profiles corresponding to other reference quiet days will fall within the shaded region. From this plot one can estimate that the neutral density increase in the thermosphere during the storm ranged from 15% at 150 altitude to about 80% at 500 km. Also, the density difference at 210 km is about 25% and it can range from 15% to 45% based on which day is being selected as the reference. For a comparison purpose the density enhancement using only the MSIS2, with F10.7 = 120 sfu and 3 hr ap = 56 nT for storm day and 8 nT for quiet day, is also shown in Figure 5d. Note that the MSIS2 only calculation underestimated the density enhancement by 44% at 200 km compared to GOLD-MSIS. It may be noted that most of the prior SpaceX launches were into an F10.7 < 100 sfu environment, and many were F10.7 < 80 sfu. So the density increase relative to those earlier launches would be much larger than 15% (at 150 km).

In addition to the MSIS-GOLD estimated density changes, that are retrieved based on the T_{eff} difference of 61 K, the MAGE model calculation of thermospheric neutral density changes are also shown in Figure 5d with a dashed line. Similar to GOLD calculations, 1 February has been used as the baseline quiet day. Also, the temporal and spatial averaging of the densities are similar to GOLD. The MAGE model calculated $\Delta\rho$ (03 and 04 February with reference to 01 February) is in good agreement with GOLD assisted MSIS2 (MSIS-GOLD) calculation. This is an interesting finding indicating that the coupled geospace MAGE model, which describes better the location and strength of Joule heating during a storm, as well as their temporal evolution (Pham et al., 2022), predicts temperature changes close to GOLD observations. These two independent calculations demonstrate that the thermospheric density increased significantly during the minor geomagnetic storm on 03–04 February 2022. Therefore, drag on the low-earth orbiting satellites would change proportionately, which could potentially be responsible for VLEO satellite deorbiting.

5. Discussion

The increased density at thermospheric altitudes has great implications on the satellite drag estimation. For a 15% increase in density it is necessary for a VLEO satellite to have sufficient thrust to overcome the drag and maintain the altitude. Even though, the current geomagnetic storm was a minor event it has impacted the density so much (about 25% at 200 km) that the corresponding drag could potentially be responsible for satellite deorbiting. Our results demonstrated that GOLD temperature observations could be inverted using a background model to infer the density changes in the thermosphere during a minor event. In the future, similar inversions could be done for moderate to extreme events using GOLD temperature, which could provide better understanding of the thermospheric density changes. If the storms are severe to extreme, they would increase the density enormously and therefore the loss could be severe (T. Fuller-Rowell et al., 2018). However, knowledge gained from rich spatio-temporal observations from GOLD could help mitigate those loses to-some-extent by simulating and selectively choosing perigee latitude, altitude, and reserve-fuel for additional thrust. For this, low-latency GOLD data could be used in an operational model to provide short term forecast in response to a space weather event. Also, there could be a possibility of operational forecast for perigee altitude for a given payload mass, reserve fuel, and space weather condition. Therefore, it is necessary to update the current empirical and forecasting models with state-of-the-art experimental measurements for a better short-term forecast capability of the thermospheric densities, particularly at LEO altitudes.

These results also indicate that GOLD T_{disk} observations can be assimilated in data assimilation and forecasting models to improve the nowcasts and forecasts. Also, the GOLD data can be used to improve the empirical models, for example, MSIS2 and assimilative models, for example, Whole Atmosphere Community Climate Model with thermosphere and ionosphere extension (Laskar, Pedatella, et al., 2021; Laskar et al., 2022), and other upper atmosphere data assimilative models (Jackson et al., 2019). As the impact of geomagnetic storms varies with latitude, an elliptic satellite with a perigee at high-latitude will have different drag compared to a low-latitude perigee. Also, for such orbits the knowledge of drag at perigee altitudes is critical as most of the heavy payload (e.g., SpaceX-Starlink launches with early phase of electric orbit raising), interplanetary (e.g., NASA's Lucy and Artemis-1 spacecrafts), and geostationary orbit missions (e.g., GOLD in SES-14) are initially launched in elliptical transfer orbits. So, it is obvious that avoidance of low-altitude and high-latitude perigee is best to be safe from effects of space weather related impacts.

6. Summary and Conclusions

Thermospheric conditions during the minor geomagnetic storm on 03 and 04 February 2022 are investigated using GOLD disk temperature measurements and simulations using MSIS2 and MAGE. The salient results are summarized below:

1. GOLD T_{disk} was about 61 K higher for the storm days compared to a pre-storm quiet time.
2. A parameterized MSIS2 simulation corresponding to the 61 K T_{eff} enhancement shows about 15% (at 150) to 80% (at 500 km) density increase.
3. T_{eff} simulated by MAGE are about 2% lower than GOLD T_{disk}. For unparameterized MSIS2 it is about 7% lower.
4. Neutral density enhancement in response to a minor storm in MAGE agrees well with GOLD assisted MSIS2 density simulations.

These results show that the even during a minor geomagnetic storm the thermospheric density and therefore the drag can be perturbed significantly. Also, it shows that the current empirical models (e.g., MSIS2) underestimate the density enhancement in response to minor events. This also demonstrates that there is a great potential of the GOLD T_{disk} to improve thermospheric density forecast models. Further investigations are needed to find out the locations and altitudes of the Starlink satellites that experienced significant increased drag and consequently reentered the atmosphere during the current storms and GOLD disk temperatures could be of great help in this regards.

Data Availability Statement

GOLD Level 2 data used in this study are available at the GOLD Science Data Center (https://gold.cs.ucf.edu/search/) and at NASA's Space Physics Data Facility (https://spdf.gsfc.nasa.gov/pub/data/gold/level2/tdisk/). The derived data products from MAGE are available at https://doi.org/10.5281/zenodo.6807766. The contribution function data for the GOLD T_{disk} are available at https://doi.org/10.5281/zenodo.7574771. The NRLMSIS 2.1 fortran language code is available at https://map.nrl.navy.mil/map/pub/nrl/NRLMSIS/NRLMSIS2.1/. For the present study a python-wrapper of this code is used from https://doi.org/10.5281/zenodo.5348502. The ap index, Dst index, IMF fields, and F10.7 flux data are obtained from NASA omniweb (https://omniweb.gsfc.nasa.gov/), which obtains data from GFZ Potsdam, Germany (Matzka et al., 2021); Space Weather Canada https://www.spaceweather.gc.ca/forecast-prevision/solar-solaire/solarflux/sx-en.php; and World Data Centre, Kyoto https://wdc.kugi.kyoto-u.ac.jp/. The 30 min cadence ap indices are obtained from https://doi.org/10.5880/HPO.0002. The two line element data used in the Supporting Information S1 are obtained from the webpage https://www.space-track.org/. The GOES-17 electron flux data are obtained from from NOAA available at https://data.ngdc.noaa.gov/platforms/solar-space-observing-satellites/goes/goes17/l1b/seis-l1b-mpsh/2022/02/.

References

Aa, E., Zhang, S.-R., Erickson, P. J., Coster, A. J., Goncharenko, L. P., Varney, R. H., & Eastes, R. (2021). Salient midlatitude ionosphere-thermosphere disturbances associated with SAPS during a minor but geo-effective storm at deep solar minimum. *Journal of Geophysical Research: Space Physics*, *126*(7), e2021JA029509. https://doi.org/10.1029/2021ja029509

Akasofu, S.-I. (1981). Energy coupling between the solar wind and the magnetosphere. *Space Science Reviews*, *28*(2), 121–190. https://doi.org/10.1007/bf00218810

Aksnes, A., Eastes, R., Budzien, S., & Dymond, K. (2006). Neutral temperatures in the lower thermosphere from N_2 Lyman-Birge-Hopfield (LBH) band profiles. *Geophysical Research Letters*, *33*(15), L15103. https://doi.org/10.1029/2006gl026255

Berger, T. E., Holzinger, M. J., Sutton, E. K., & Thayer, J. P. (2020). Flying through uncertainty. *Space Weather*, *18*(1), e2019SW002373. https://doi.org/10.1029/2019sw002373

Borovsky, J. E., & Shprits, Y. Y. (2017). Is the *Dst* index sufficient to define all geospace storms? *Journal of Geophysical Research: Space Physics*, *122*(11), 11543–11547. https://doi.org/10.1002/2017ja024679

Bruinsma, S., Forbes, J. M., Nerem, R. S., & Zhang, X. (2006). Thermosphere density response to the 20–21 November 2003 solar and geomagnetic storm from CHAMP and GRACE accelerometer data. *Journal of Geophysical Research*, *111*(A6), A06303. https://doi.org/10.1029/2005ja011284

Burns, A. G., Killeen, T. L., Deng, W., Carignan, G. R., & Roble, R. G. (1995). Geomagnetic storm effects in the low- to middle-latitude upper thermosphere. *Journal of Geophysical Research*, *100*(A8), 14673. https://doi.org/10.1029/94ja03232

Cai, X., Burns, A. G., Wang, W., Qian, L., Pedatella, N., Coster, A., et al. (2021). Variations in thermosphere composition and ionosphere total electron content under "geomagnetically quiet" conditions at solar-minimum. *Geophysical Research Letters*, *48*(11), e2021GL093300. https://doi.org/10.1029/2021gl093300

Cai, X., Burns, A. G., Wang, W., Qian, L., Solomon, S. C., Eastes, R. W., et al. (2021). Investigation of a neutral "tongue" observed by GOLD during the geomagnetic storm on May 11, 2019. *Journal of Geophysical Research: Space Physics*, *126*(6), e2020JA028817. https://doi.org/10.1029/2020ja028817

Crowley, G., Hackert, C. L., Meier, R. R., Strickland, D. J., Paxton, L. J., Pi, X., et al. (2006). Global thermosphere-ionosphere response to onset of 20 November 2003 magnetic storm. *Journal of Geophysical Research*, *111*(A10), A10S18. https://doi.org/10.1029/2005ja011518

Dang, T., Li, X., Luo, B., Li, R., Zhang, B., Pham, K., et al. (2022). Unveiling the space weather during the starlink satellites destruction event on 4 February 2022. *Space Weather*, *20*(8), e2022SW003152. https://doi.org/10.1029/2022sw003152

Eastes, R. W., McClintock, W. E., Burns, A. G., Anderson, D. N., Andersson, L., Aryal, S., et al. (2020). Initial observations by the GOLD mission. *Journal of Geophysical Research: Space Physics*, *125*(7), e2020JA027823. https://doi.org/10.1029/2020ja027823

Eastes, R. W., Solomon, S. C., Daniell, R. E., Anderson, D. N., Burns, A. G., England, S. L., et al. (2019). Global-scale observations of the equatorial ionization anomaly. *Geophysical Research Letters*, *46*(16), 9318–9326. https://doi.org/10.1029/2019gl084199

Eastwood, J. P., Biffis, E., Hapgood, M. A., Green, L., Bisi, M. M., Bentley, R. D., et al. (2017). The economic impact of space weather: Where do we stand? *Risk Analysis*, *37*(2), 206–218. https://doi.org/10.1111/risa.12765

Emmert, J. T., Drob, D. P., Picone, J. M., Siskind, D. E., Jones, M., Mlynczak, M. G., et al. (2021). NRLMSIS 2.0: A whole-atmosphere empirical model of temperature and neutral species densities. *Earth and Space Science*, *8*(3), e2020EA001321. https://doi.org/10.1029/2020ea001321

Emmert, J. T., Jones, M., Siskind, D. E., Drob, D. P., Picone, J. M., Stevens, M. H., et al. (2022). NRLMSIS 2.1: An empirical model of nitric oxide incorporated into MSIS. *Journal of Geophysical Research: Space Physics*, *127*(10), e2022JA030896. https://doi.org/10.1029/2022ja030896

Evans, J. S., Eastes, R., Lumpe, J. D., Correira, J., Burns, A. G., McClintock, B., et al. (2018). Global-scale observations of the limb and disk (GOLD): Overview of daytime neutral temperature science data product. In *Agu fall meeting abstracts*, (Vol. 2018, p. SA21A-3172).

Forbes, J. M., Gonzalez, R., Marcos, F. A., Revelle, D., & Parish, H. (1996). Magnetic storm response of lower thermosphere density. *Journal of Geophysical Research*, *101*(A2), 2313–2319. https://doi.org/10.1029/95ja02721

Fuller-Rowell, T., Emmert, J., Fedrizzi, M., Weimer, D., Codrescu, M. V., Pilinski, M., et al. (2018). How might the thermosphere and ionosphere react to an extreme space weather event? In *Extreme events in geospace* (pp. 513–539). Elsevier. https://doi.org/10.1016/b978-0-12-812700-1.00021-2

Fuller-Rowell, T. J., Codrescu, M. V., Moffett, R. J., & Quegan, S. (1994). Response of the thermosphere and ionosphere to geomagnetic storms. *Journal of Geophysical Research*, *99*(A3), 3893. https://doi.org/10.1029/93ja02015

Hapgood, M., Liu, H., & Lugaz, N. (2022). SpaceX—Sailing close to the space weather? *Space Weather*, *20*(3), e2022SW003074. https://doi.org/10.1029/2022sw003074

Hedin, A. E. (1987). MSIS-86 thermospheric model. *Journal of Geophysical Research*, *92*(A5), 4649. https://doi.org/10.1029/ja092ia05p04649

Hedin, A. E. (1991). Extension of the MSIS thermosphere model into the middle and lower atmosphere. *Journal of Geophysical Research*, *96*(A2), 1159–1172. https://doi.org/10.1029/90ja02125

Jackson, D. R., Fuller-Rowell, T. J., Griffin, D. J., Griffith, M. J., Kelly, C. W., Marsh, D. R., & Walach, M.-T. (2019). Future directions for whole atmosphere modeling: Developments in the context of space weather. *Space Weather*, *17*(9), 1342–1350. https://doi.org/10.1029/2019sw002267

Knipp, D. J., Pette, D. V., Kilcommons, L. M., Isaacs, T. L., Cruz, A. A., Mlynczak, M. G., et al. (2017). Thermospheric nitric oxide response to shock-led storms. *Space Weather*, *15*(2), 325–342. https://doi.org/10.1002/2016sw001567

Krywonos, A., Murray, D. J., Eastes, R. W., Aksnes, A., Budzien, S. A., & Daniell, R. E. (2012). Remote sensing of neutral temperatures in the Earth's thermosphere using the Lyman-Birge-Hopfield bands of N_2: Comparisons with satellite drag data. *Journal of Geophysical Research*, *117*(A9), A09311. https://doi.org/10.1029/2011ja017226

Laskar, F. I., Eastes, R. W., Codrescu, M. V., Evans, J. S., Burns, A. G., Wang, W., et al. (2021). Response of GOLD retrieved thermospheric temperatures to geomagnetic activities of varying magnitudes. *Geophysical Research Letters*, *48*(15), e2021GL093905. https://doi.org/10.1029/2021gl093905

Laskar, F. I., Eastes, R. W., Martinis, C. R., Daniell, R. E., Pedatella, N. M., Burns, A. G., et al. (2020). Early morning equatorial ionization anomaly from GOLD observations. *Journal of Geophysical Research: Space Physics*, *125*(7), e2019JA027487. https://doi.org/10.1029/2019ja027487

Laskar, F. I., Pedatella, N. M., Codrescu, M. V., Eastes, R. W., Evans, J. S., Burns, A. G., & McClintock, W. (2021). Impact of GOLD retrieved thermospheric temperatures on a whole atmosphere data assimilation model. *Journal of Geophysical Research: Space Physics*, *126*(1), e2020JA028646. https://doi.org/10.1029/2020ja028646

Laskar, F. I., Pedatella, N. M., Codrescu, M. V., Eastes, R. W., & McClintock, W. E. (2022). Improving the thermosphere ionosphere in a whole atmosphere model by assimilating GOLD disk temperatures. *Journal of Geophysical Research: Space Physics*, *127*(3), e2021JA030045. https://doi.org/10.1029/2021ja030045

Li, R., & Lei, J. (2021). Responses of thermospheric mass densities to the October 2016 and September 2017 geomagnetic storms revealed from multiple satellite observations. *Journal of Geophysical Research: Space Physics*, *126*(1), e2020JA028534. https://doi.org/10.1029/2020ja028534

Lin, D., Sorathia, K., Wang, W., Merkin, V., Bao, S., Pham, K., et al. (2021). The role of diffuse electron precipitation in the formation of subauroral polarization streams. *Journal of Geophysical Research: Space Physics*, *126*(12), e2021JA029792. https://doi.org/10.1029/2021ja029792

Lin, D., Wang, W., Garcia-Sage, K., Yue, J., Merkin, V., McInerney, J. M., et al. (2022). Thermospheric neutral density variation during the "SpaceX" storm: Implications from physics-based whole geospace modeling. *Space Weather*, *20*(12), e2022SW003254. https://doi.org/10.1029/2022sw003254

Lin, D., Wang, W., Merkin, V. G., Huang, C., Oppenheim, M., Sorathia, K., et al. (2022). Origin of dawnside subauroral polarization streams during major geomagnetic storms. *AGU Advances*, *3*(4), e2022AV000708. https://doi.org/10.1029/2022av000708

Liu, H., & Lühr, H. (2005). Strong disturbance of the upper thermospheric density due to magnetic storms: CHAMP observations. *Journal of Geophysical Research*, *110*(A9), A09S29. https://doi.org/10.1029/2004ja010908

Liu, R., Lühr, H., & Ma, S.-Y. (2010). Storm-time related mass density anomalies in the polar cap as observed by CHAMP. *Annales Geophysicae*, *28*(1), 165–180. https://doi.org/10.5194/angeo-28-165-2010

Loewe, C. A., & Prölss, G. W. (1997). Classification and mean behavior of magnetic storms. *Journal of Geophysical Research*, *102*(A7), 14209–14213. https://doi.org/10.1029/96ja04020

Lucas, G. (2021). pymsis. [Computer software]. Zenodo. Retrieved from https://swx-trec.com/msis/about

Lumpe, J. D., Bevilacqua, R. M., Hoppel, K. W., & Randall, C. E. (2002). POAM III retrieval algorithm and error analysis. *Journal of Geophysical Research*, *107*(D21), ACH 5-1–ACH 5-32. https://doi.org/10.1029/2002jd002137

Matzka, J., Bronkalla, O., Kervalishvili, G., Rauberg, J., & Yamazaki, Y. (2022). *Geomagnetic hpo index*. GFZ Data Services. Retrieved from https://www.gfz-potsdam.de/hpo-index/

Matzka, J., Stolle, C., Yamazaki, Y., Bronkalla, O., & Morschhauser, A. (2021). The geomagnetic Kp index and derived indices of geomagnetic activity. *Space Weather*, *19*(5), e2020SW002641. https://doi.org/10.1029/2020sw002641

McClintock, W. E., Eastes, R. W., Beland, S., Bryant, K. B., Burns, A. G., Correira, J., et al. (2020). Global-scale observations of the limb and disk mission implementation: 2. Observations, data pipeline, and level 1 data products. *Journal of Geophysical Research: Space Physics*, *125*(5), e2020JA027809. https://doi.org/10.1029/2020ja027809

McPherron, R. L., & Chu, X. (2016). The mid-latitude positive bay and the MPB index of substorm activity. *Space Science Reviews*, *206*(1–4), 91–122. https://doi.org/10.1007/s11214-016-0316-6

Merkin, V. G., & Lyon, J. G. (2010). Effects of the low-latitude ionospheric boundary condition on the global magnetosphere. *Journal of Geophysical Research*, *115*(A10), A10202. https://doi.org/10.1029/2010ja015461

Mlynczak, M. G., Knipp, D. J., Hunt, L. A., Gaebler, J., Matsuo, T., Kilcommons, L. M., & Young, C. L. (2018). Space-based sentinels for measurement of infrared cooling in the thermosphere for space weather nowcasting and forecasting. *Space Weather*, *16*(4), 363–375. https://doi.org/10.1002/2017sw001757

Oliveira, D. M., & Zesta, E. (2019). Satellite orbital drag during magnetic storms. *Space Weather*, *17*(11), 1510–1533. https://doi.org/10.1029/2019sw002287

Pham, K. H., Zhang, B., Sorathia, K., Dang, T., Wang, W., Merkin, V., et al. (2022). Thermospheric density perturbations produced by traveling atmospheric disturbances during August 2005 storm. *Journal of Geophysical Research: Space Physics*, *127*(2), e2021JA030071. https://doi.org/10.1029/2021ja030071

Picone, J. M., Hedin, A. E., Drob, D. P., & Aikin, A. C. (2002). NRLMSISE-00 empirical model of the atmosphere: Statistical comparisons and scientific issues. *Journal of Geophysical Research*, *107*(A12), SIA 15-1–SIA 15-16. https://doi.org/10.1029/2002ja009430

Prölss, G. W. (2010). Density perturbations in the upper atmosphere caused by the dissipation of solar wind energy. *Surveys in Geophysics*, *32*(2), 101–195. https://doi.org/10.1007/s10712-010-9104-0

Qian, L., Burns, A. G., Emery, B. A., Foster, B., Lu, G., Maute, A., et al. (2014). The NCAR TIE-GCM. In *Modeling the ionosphere-thermosphere system* (pp. 73–83). John Wiley & Sons, Ltd. https://doi.org/10.1002/9781118704417.ch7

Qian, W., Dong, L., Wenbin, W., & William, W. (2022). Thermospheric wind observation and simulation during the Nov 4, 2021 geomagnetic storm event. *Journal of Astronomy and Space Sciences*, *39*(3), 79–86.

Richmond, A. D. (2021). Joule heating in the thermosphere. In *Upper atmosphere dynamics and energetics* (pp. 1–18). American Geophysical Union (AGU). https://doi.org/10.1002/9781119815631.ch1

Richmond, A. D., & Lu, G. (2000). Upper-atmospheric effects of magnetic storms: A brief tutorial. *Journal of Atmospheric and Solar-Terrestrial Physics*, *62*(12), 1115–1127. https://doi.org/10.1016/s1364-6826(00)00094-8

Richmond, A. D., Ridley, E. C., & Roble, R. G. (1992). A thermosphere/ionosphere general circulation model with coupled electrodynamics. *Geophysical Research Letters*, *19*(6), 601–604. https://doi.org/10.1029/92gl00401

Rodgers, C. D. (2000). *Inverse methods for atmospheric sounding*. WORLD SCIENTIFIC. https://doi.org/10.1142/3171

Shi, X., Lin, D., Wang, W., Baker, J. B. H., Weygand, J. M., Hartinger, M. D., et al. (2022). Geospace concussion: Global reversal of ionospheric vertical plasma drift in response to a sudden commencement. *Geophysical Research Letters*, *49*(19), e2022GL100014. https://doi.org/10.1029/2022gl100014

Sorathia, K. A., Merkin, V. G., Panov, E. V., Zhang, B., Lyon, J. G., Garretson, J., et al. (2020). Ballooning-interchange instability in the near-earth plasma sheet and auroral beads: Global magnetospheric modeling at the limit of the MHD approximation. *Geophysical Research Letters*, *47*(14), e2020GL088227. https://doi.org/10.1029/2020gl088227

Sutton, E. K., Forbes, J. M., & Knipp, D. J. (2009). Rapid response of the thermosphere to variations in joule heating. *Journal of Geophysical Research*, *114*(A4), A04319. https://doi.org/10.1029/2008ja013667

Sutton, E. K., Forbes, J. M., & Nerem, R. S. (2005). Global thermospheric neutral density and wind response to the severe 2003 geomagnetic storms from CHAMP accelerometer data. *Journal of Geophysical Research*, *110*(A9), A09S40. https://doi.org/10.1029/2004ja010985

Toffoletto, F., Sazykin, S., Spiro, R., & Wolf, R. (2003). Inner magnetospheric modeling with the rice convection model. *Space Science Reviews*, *107*(1/2), 175–196. https://doi.org/10.1023/a:1025532008047

Yamazaki, Y., Matzka, J., Stolle, C., Kervalishvili, G., Rauberg, J., Bronkalla, O., et al. (2022). Geomagnetic activity index Hpo. *Geophysical Research Letters*, *49*(10), e2022GL098860. https://doi.org/10.1029/2022gl098860

Yuan, L., Jin, S., & Calabia, A. (2019). Distinct thermospheric mass density variations following the September 2017 geomagnetic storm from GRACE and Swarm. *Journal of Atmospheric and Solar-Terrestrial Physics*, *184*, 30–36. https://doi.org/10.1016/j.jastp.2019.01.007

Zesta, E., & Oliveira, D. M. (2019). Thermospheric heating and cooling times during geomagnetic storms, including extreme events. *Geophysical Research Letters*, *46*(22), 12739–12746. https://doi.org/10.1029/2019gl085120